Indian Journal of Chemistry
Vol. 64, April 2025, pp. 411-426
DOI: 10.56042/ijc.v64i4.17187

# Virtual screening, molecular docking, MD simulation, MMPBSA, and DFT analysis of marine drugs in search of molecules effective against KRAS mutation

Supriyo Saha*[a], Mahima Singh[a], Prinsa[b] & Vikash Jakhmola[a]

[a] Department of Pharmaceutical Chemistry, Uttaranchal Institute of Pharmaceutical Sciences, Uttaranchal University, Dehradun 248 007, Uttarakhand, India

[b] Department of Pharmaceutical Chemistry, Siddhartha Institute of Pharmacy, Near IT-Park, Sahastradhara Road, Dehradun 248 001, Uttarakhand, India

E-mail: supriyo9@gmail.com

*Received: 15 February 2025; accepted (revised) 24 March 2025*

Marine bioactive compounds have been showing diversified bioactivities such as antifungal, antimicrobial, anticancer, and antiviral. Mutations of KRAS G12C and G12D protooncogenes are responsible for colorectal, lung, and pancreatic cancers. KRAS G12C and G12D inhibitors sotorasib, MRTX 1133, and adagrasib showed good anticancer potential. In this research, we have screened 2000 marine bioactive compouds from marine database and 1699 molecules show highest probability as drug like structure. Selected marine compounds have been molecular docked against KRAS G12C and G12D using sotorasib and MRTX 1133 as standard structures. In case of KRAS G12C inhibition, Halenaquinone, xestoquinone, halenaquinol, and sotorasib show good docking scores of –11.7 kcal/mol, –11.6 kcal/mol, 11.5 kcal/mol, and –9.1 kcal/mol, respectively. In case of KRAS G12D inhibition Pseudane V, 1,6,10-trihydroxy-8-methyltetracene-5,12-dione, Methylaplysinopsine, and MRTX 1133 show good docking scores of –11.0 kcal/mol, –9.9 kcal/mol, and 9.7 kcal/mol, and –10.2 kcal/mol, respectively. MD simulation and MMPBSA analysis data show that RMSD, RMSF, SASA, Rg and hydrogen bond analysis reflect the structural integrity and stability of drug-receptor complex. FMO analysis shows that Xestoquinone and 1,6,10-trihydroxy-8-methyltetracene-5,12-dione represent soft molecules effective against KRAS G12C and G12D, respectively. This research confirmed the potential of marine ecosystem in the management of cancer by targeting KRAS mutations.

**Keywords:** Marine bioactive compounds, KRAS, Molecular docking, MD simulation, DFT

KRAS is a proto-oncogene that plays a crucial role in regulating cell division, growth, and differentiation[1,2]. It encodes a protein that belongs to the RAS family of small GTPase, which act as molecular switches within cells. When KRAS is functioning normally, it helps control these cellular processes by cycling between an active and inactive state[3,4]. However, mutations in the KRAS gene can lead to uncontrolled cell growth and are commonly associated with various cancers, including pancreatic, lung, and colorectal cancers[5,6]. These mutations often result in a permanently active form of the KRAS protein, which continually signals cells to divide and grow, contributing to tumor development. These mutations cause the KRAS protein to be constitutively active, or always in the "on" state[7,8]. This continuous activation promotes unchecked cell growth, which is a common cause of cancer[9,10]. The following are the most common KRAS mutations: G12D: Position 12: Aspartic acid to glycine[11]. The KRAS gene and protein in their typical, unaltered state is known as Wild-Type KRAS. In cells containing wild-type KRAS, the protein functions as intended and its activity is tightly regulated[12]. The following are the three main KRAS isoforms that arise from alternative splicing: KRAS4A: Exon 4A is the source. G12V: Glycine to valine at position 12, G13D: Glycine to aspartic acid at position 13, Q61H: Glutamine to histidine at position 61, Q61L: Glutamine to leucine at position 61[13]. Wild-Type KRAS: This refers to the normal, unmutated form of the KRAS gene and protein[14]. In cells with wild-type KRAS, the protein functions properly and its activity is tightly regulated. KRAS isoforms: KRAS exists in multiple isoforms due to alternative splicing, with the main ones being: KRAS4A: Produced from exon 4A. KRAS4B: Produced from exon 4B[15,16]. Both isoforms have similar functions but may differ in their interactions with other proteins and their roles in various tissues[17].

KRAS variants: There are various less-common mutations and polymorphisms that can occur in KRAS, though these are less well-characterized compared to the primary oncogenic mutations[18]. Sotorasib, adagrasib, and MRTX 849 specifically targets the KRAS G12C mutant and showed good inhibition of non-small lung and colorectal cancers. GDC-6306 is the new molecule with KRAS G12D and G12V inhibitors[19]. Trametinib and cobimetinib are the KRAS effectors which inhibited MEK/ERK pathways[20]. Marine drugs are increasingly used in drug discovery such as anticancer drugs, antimicrobial agents also used as cosmetics, nutraceuticals and in biotechnology. Biodiversity of marine drugs refers to the wide range of chemical compounds produced by marine organisms, which have significant pharmacological activities in human and animal bodies[21]. Bryostatin-1, known for its immune-modulating properties, has been isolated and its mechanism of action involves the activation of protein kinase C, which mediates cell signal transduction pathways[22]. Marine microorganisms including phytoplankton represent a significant reservoir of bioactive compounds with potential therapeutic applications[23]. Marine bacteria actinomycetes under the genus Salinispora observed with antibiotic properties and micromonospora including gentamicin, an antibiotic effective in the treatment of bacterial infections[24,25]. Marine cyanobacteria organisms generate a diverse array of secondary metabolites, such as curacin A, which is recognized for its anticancer properties[26,27]. Vibrio species of marine bacteria showed good activity in the treatment of infections. Marine fungi species such as Aspergillus and Penicillium played a vital role in the treatment of numerous bacterial infections[28]. Eurotium and Talaromyces are responsible for antiviral and anticancer activities. Cladosporium genus possess with anti-inflammatory properties[29,30]. In this research, we try to establish the role of marine drugs in the inhibition of KRAS G12C and G12D using Virtual Screening, Molecular Docking, MD Simulation, MMPBSA, Principal component analysis, Gibbs Energy Landscape, Density Functional Theory (DFT), Principal Component Analysis, and ADMET Analyses.

## Experimental Details

### Virtual Screening and Assessment of Drug like Property

In this work 2000 marine based compounds were obtained from marine database (https://www.cmnpd.org/) and passed through drug like parameter (Lipinski rule of five). Here marine compounds were obtained from marine algae, coral, marine bacteria, marine fungi, marine sponges, cnidarians, bryozoans, moluscus, ascidians, and echinoderms. Drug like property (Lipinski rule of five) display the ability of a chemical structure to behave like a drug molecule. Lipinski rule of five expressed that if a chemical structure observed with molecular mass not more than 500 dalton, hydrogen bond donor group not more than 5, hydrogen bond acceptor group not more than 10, and partition coefficient value of the structure not more than 5. In this work Lipinski rule of five was considered as primary filter to identify drug like marine compounds (Table S1). Out of the 2000 marine compounds, 1699 molecules finally passed the primary filter and these molecules were selected for further computational studies.

## Molecular Docking Study using AutoDock Vina

### Preparation of protein

In this work we considered KRAS G12C receptor complexed with LXD (PDB id: 8AFB) and KRAS G12D receptor complexed with 7L8 (PDB id: 7RT1) for molecular docking analysis of selected 1699 marine drugs[31,32]. KRAS G12C receptor was comprised of one chain with 170 amino acids. Inside the receptor, complexed ligand LXD was connected with GLU 63, ARG 68, ASP 69, TYR 64, MET 72, VAL 103, CYS 12, GLU 62, ASP 92, and HIS 95. Ramachandran plot of KRAS G12C and G12D receptors showed 92.6%, 6.8%, 0.7%, 0.0% and 94.1%, 5.9%, 0.0%, 0.0% residues comes under most favored, additional allowed, generously allowed regions, and disallowed regions, respectively (Fig. S2 and S3) [33]. In KRAS G12D receptor, one chain with 170 amino acids were present and the complexed ligand 7L8 connected with TYR 64, ARG 68, ASP 69, MET 72, ASP 12, GLY 60, GLU 62, VAL 103, and HIS 95 (Fig. S1). As per verify3d server of KRAS G12C and G12D receptors, 86.59% and 85.80% of the residues have average 3D-1D score greater than 0.1 which showed that amino acid residues present in the receptors associated with protein quality for modeling[34]. Overall quality value of the KRAS G12C and G12D receptors as per ERRAT were 94.87, and 98.75, which showed good resolution (Fig. S2). The VoRoMQA analysis data of KRAS G12C and G12D receptors showed 0.510, and 0.525 revealed that protein structures were good for

analysis. If VoRoMQA score greater than 0.4, then the model was likely good, score less than 0.3, model was likely bad and if score was between 0.3 and 0.4, model cannot be reliably classified as either good or bad (Fig. S3)[35]. After removing the complexed ligands, water molecules, receptors were modeled through Autodock Tools 1.5.6 for the addition of polar hydrogen and gasteiger charge. Finally, the structures of the receptors were saved into pdbqt format.

**Preparation of marine drugs structures for molecular docking**

Avogadro software was used to draw the structures of selected marine drugs, sotorasib, and MRTX 1133 followed by force field- based energy minimization. All the structures were saved in pdb format. Then by using Autodock Tools 1.5.6 all the structures were subjected to addition of gasteiger charge and polar hydrogen. Finally, the structures were saved into docking feasible pdbqt format[36].

**Preparation of grid box**

By identifying the interactive amino acid residues, the grid box dimension of KRAS G12C and G12D receptors were obtained in x, y and z axis, which was center_x=18.479, center_y=−8.144, center_z=22.453; and center_x=−1.527, center_y=0.218, center_z=−21.073 with size_x=24, size_y=24, size_z=24 and exhaustiveness = 8, respectively[37].

**Visualization and validation of docking results**

Biovia Drug Discovery Studio visualizer was used to visualize the molecular docking interactions and Root mean square deviation (RMSD) values were calculated by removing the complexed ligands and redocked again within the receptor active site[38].

**Molecular Dynamic (MD) Simulation of the selected Marine Bioactive Compounds**

Here, top3 docked compounds (CMNPD 1953, CMNPD 1955, CMNPD 1956) and (CMNPD 238, CMNPD 965, and CMNPD 1749) which showed good interactions against KRAS G12C and G12D, respectively were chosen for 100 ns MD simulation. MD simulation showcased the atomic level interactions of a ligand molecule within the receptor active site in presence of solvent, pressure, temperature, and ions[39]. Here GROMACS 20.1 software package was utilized to perform the MD simulation analysis. In the first step, the protein-ligand complex was transferred into GROMACS environment and removes the complexed ligand from the complex. Then CHARMM force field and TIP3 solvents were added in the receptor. Then both receptor and ligand were saved in GROMACS accessible gro format and also topology file was generated. In case of CMNPD 1953, CMNPD 1955, and CMNPD 1956: 6561, 7254, 8386 water molecules and 7, 7, 7 sodium ions were added in the topology files, respectively. In case of CMNPD 238, CMNPD 965, and CMNPD 1749: 6512, 6510, 6504 water molecules and 7, 7, 7 sodium ions were added in the topology files, respectively. Then the energy of the receptor-ligand complex was minimized, and the complex was equilibrated in terms of temperature, volume, and pressure[40]. After completion of simulation root mean square standard deviations and fluctuations were determined for every receptor-ligand complex to identify the nature of interaction and amino acid residues during interaction. Also, the receptor-ligand complex stability was identified by radius of gyration and solvent accessible surface area calculation. MD simulation analysis data was reported in comparison with apoenzyme, and sotorasib (standard for KRAS G12C) and MRTX 1133 (standard for KRAS G12D). QtGrace software was used to analyze the simulation trajectories[41].

**MMPBSA Analysis**

Molecular Mechanics Poisson-Boltzmann Surface Area (MMPBSA) analysis was used to determine the free binding energies of the receptor-ligand complex based on van der waal, electrostatic, polar salvation, and SASA energies[42].

**Density Functional Theory Analyses**

**Frontier Molecular Orbital (FMO) Analysis**

Electronic behaviour of CMNPD 238, CMNPD 965, CMNPD 1749, CMNPD 1953, CMNPD 1955, and CMNPD 1956 were determined by Beck's (B) three-parameter hybrid model and Lee, Yang, and Parr's (LYP) correlation functional under the B3LYP/6-31G (d,p) basis set. Highest occupied molecular orbital and lowest unoccupied molecular orbital energies and the gaps between these two orbitals were calculated and the data was associated with softness, electronegativity, hardness, and electrophilicity properties of the structures. GAMESS software and WxMacMolPlt (version 7.7.3) were used for FMO analysis[43].

Chemical hardness: $\eta = \frac{I-A}{2}$; softness: $\zeta = \frac{1}{2\eta}$; electronegativity: $\mu = -\frac{I+A}{2}$; electrophilicity index: $\Psi = \frac{\mu 2}{2\eta}$; where A and I are electron affinity and ionization potential. $A = -E_{LUMO}$ and $I = -E_{HOMO}$.

**Molecular Electrostatic Potential (MEP) Analysis**

MEP map analysis was also performed by Beck's (B) three-parameter hybrid model and Lee, Yang, and Parr's (LYP) correlation functional under the B3LYP/6-31G (d,p) basis set to identify the possible zones/functional group for electrophilic and nucleophilic attack using GAMESS software (version R2 released on June 30, 2024) with B3LYP/6-31G(d,p) to identify the MEP analysis. Different colors in electrostatic map represent different zone in structure such as red, orange, and yellow linked with electrophilic behavior and blue linked with nucleophilic and green hue associated with neutral zone[44].

**Principal Component Analysis and Free Energy Landscape Analysis**

Principal Component Analysis (PCA) based on covariance-matrix which considers data projection in an eigenspace to identify the directions of maximum variation in data. PCA can decrease the complexity of a multidimensional set of variables to a lower dimension. This can be utilized to identify diffusive properties during the entire protein folding process[45]. A protein's free energy landscape (FEL), a high-dimensional hypersurface, described how a protein's energy changes as its structure changes. Understanding the stability and dynamics of proteins required an understanding of FEL. PCA and FEL analysis performed for CMNPD 1953-KRAS G12C, CMNPD 1955-KRAS G12C, CMNPD 1956-KRAS G12C, CMNPD 238-KRAS G12D, CMNPD 965-KRAS G12D, CMNPD 1749-KRAS G12D complexes[46].

**ADMET Analysis**

ADME (Absorption, Distribution, Metabolism, and Excretion) and toxicity properties of selected 1699 marine drugs were calculated using Swiss ADME portal and OSIRIS software, respectively[47].

**Results and Discussion**

**Molecular Docking Study Data**

Molecular docking scores of selected 1699 marine based compounds against KRAS G12C receptor were fluctuated between –4.9 kcal/mol to –11.7 kca/mol. CMNPD 1955, CMNPD 1956, and CMNPD 1953 were the top 3 molecules showed good docking interaction scores of –11.7 kcal/mol, –11.6 kcal/mol, and 11.5 kcal/mol, respectively with KRAS G12C receptor (Table S2). Standard sotorasib and complexed LXD showed molecular docking interaction scores of –9.1 kcal/mol, and –11.0 kcal/mol, respectively[36]. CMNPD 1955 (Halenaquinone) interacted with KRAS G12C receptor *via* GLY 10 (3.61 Å), LYS 16 (5.40 Å), THR 58 (4.25 Å) (hydrogen bond interaction); CYS 12 (7.91 Å) (pi-sulfur); ARG 68 (5.96 Å and 7.43 Å) by (pi-cation); MET 72 (4.72 Å) and VAL 103 (5.28 Å) (Pi-Alkyl interaction); VAL 9 (4.23 Å), GLU 62 (4.08 Å), TYR 96 (5.45 Å), ILE 100 (3.98 Å) (Pi-Hydrogen bond donor); and ALA 59, GLN 61, GLU 63, TYR 64, GLN 99, and ARG 102 (van der waals interactions). CMNPD 1956 (Xestoquinone) interacted with KRAS G12C receptor *via* GLY 10 (3.52 Å), LYS 16 (5.59 Å) (hydrogen bond interaction); CYS 12 (8.27 Å) (pi-sulfur); ARG 68 (5.79 Å and 7.31 Å) by (pi-cation); MET 72 (4.83 Å), ILE 100 (3.98 Å), and VAL 103 (4.93 Å) (Pi-Alkyl interaction); GLU 62 (4.08 Å), TYR 96 (5.45 Å), ILE 100 (3.98 Å) (Pi-Hydrogen bond donor); and ALA 59, GLN 61, GLU 63, TYR 64, ASP 69, GLN 99, and ARG 102 (van der waals interactions). CMNPD 1953 (Halenaquinol) interacted with KRAS G12C receptor *via* GLY 10 (2.60 Å), THR 58 (4.52 Å), GLU 63 (4.96 Å) (hydrogen bond interaction); CYS 12 (7.59 Å) (pi-sulfur); ARG 68 (5.82 Å and 7.50 Å) by (pi-cation); MET 72 (4.92 Å) (Pi-Alkyl interaction); GLU 62 (4.96 Å), ASP 69 (5.18 Å), TYR 96 (5.69 Å) (Pi-Hydrogen bond donor); and ALA 59, GLN 61, TYR 64, GLN 99, ILE 100, ARG 102, VAL 103 (van der waals interactions). Standard sotorasib interacted with KRAS G12C receptor *via* GLU 62 (3.91 Å), ARG 68 (3.86 Å) (hydrogen bond interaction); CYS 12 (4.47 Å), MET 72 (4.64 Å), VAL 9 (5.17 Å), TYR 96 (5.30 Å) (Pi-Alkyl interaction); GLU 62 (5.09 Å), and ASP 92 (4.46 Å) by halogen (fluorine) bond; GLU 62 (3.91 Å) by Pi-Anion bond; and ALA 59, GLN 61, TYR 64 (van der waals interactions). Complexed ligand LXD redocked with KRAS G12C receptor *via* GLU 63 (5.47 Å), ARG 68 (4.49 Å), ASP 69 (4.26 Å) by hydrogen bond interaction; GLU 62 (6.97 Å), ASP 92 (6.54 Å) by Pi-anion interaction; TYR 64 (6.96 Å) by Pi-Pi stack interaction; CYS 12 (6.45 Å), HIS 95 (4.32 Å), VAL 103 (5.59 Å) by Pi-alkyl interaction; MET 72 (5.53 Å) by Pi-sigma

interaction; and VAL 9, THR 58, ALA 59, GLN 61, GLN 99, ILE by van der waals interactions (Fig. 1). The common interacting residues between complexed ligand, best docked molecules and standard sotorasib confirmed that molecules were effectively docked within the receptor active site. Molecular docking scores of selected 1699 marine based compounds against KRAS G12D receptor were fluctuated between (–4.5 to –11.0) kcal/mol. CMNPD 238, CMNPD 1749, CMNPD 965 were the top3 molecules showed good docking interaction scores of –11.0 kcal/mol, –9.9 kcal/mol, and 9.7 kcal/mol, respectively with KRAS G12C receptor (Table S3). Standard MRTX 1133 and complexed 7L8 showed molecular docking interaction scores of –10.2 kcal/mol, and –10.7 kcal/mol, respectively[48]. CMNPD 238 (Pseudane V) interacted with KRAS G12D receptor *via* SER 39 (4.35 Å), ASP 54 (4.91 Å) (hydrogen bond interaction); LEU 5 (4.74 Å), LEU 56 (5.04 Å), TYR 71 (6.51 Å) (Pi-Alkyl interaction); and GLU 37, and ASP 38 (van der waals interactions). CMNPD 1749 (1,6,10-trihydroxy-8-methyltetracene-5,12-dione) interacted with KRAS G12D receptor *via* GLY 10 (2.56 Å), THR 58 (4.20 Å), GLN 61 (6.23 Å) by (hydrogen bond interaction); ARG 68 (5.83 Å, 6.12 Å, and 7.35 Å) by (pi-cation); MET 72 (4.80 Å) (Pi-sigma interaction); VAL 103 (6.87 Å) (Pi-alkyl interaction); and ALA 59, GLU 62, TYR 64, ASP 69, GLN 99, ILE 100, and ARG 102 by (van der waals interactions). CMNPD 965 (Methylaplysinopsine) interacted with KRAS G12D receptor *via* ARG 68 (5.96 Å) (hydrogen bond interaction); MET 72 (5.47 Å and 6.40 Å) by (Pi-Alkyl interaction); TYR 96 (5.85 Å) (Pi-Pi T shaped interaction); ALA 59 (5.23 Å), GLY 60 (4.96 Å), GLN 61 (6.65 Å) by carbon-hydrogen bond; and THR 58, GLU 62, GLU 63, TYR 64, HIS 95, GLN 99, ILE 100, VAL 103 (van der waals interactions) [49]. Standard MRTX 1133 interacted with KRAS G12D receptor *via* GLY 10 (4.26 Å), TYR 64 (4.36 Å), ARG 68 (4.99 Å), ASP 69 (3.19 Å) by (hydrogen bond interaction); ARG 102 (6.48 Å) (Pi-Cation interaction); ALA 59 (4.04 Å),

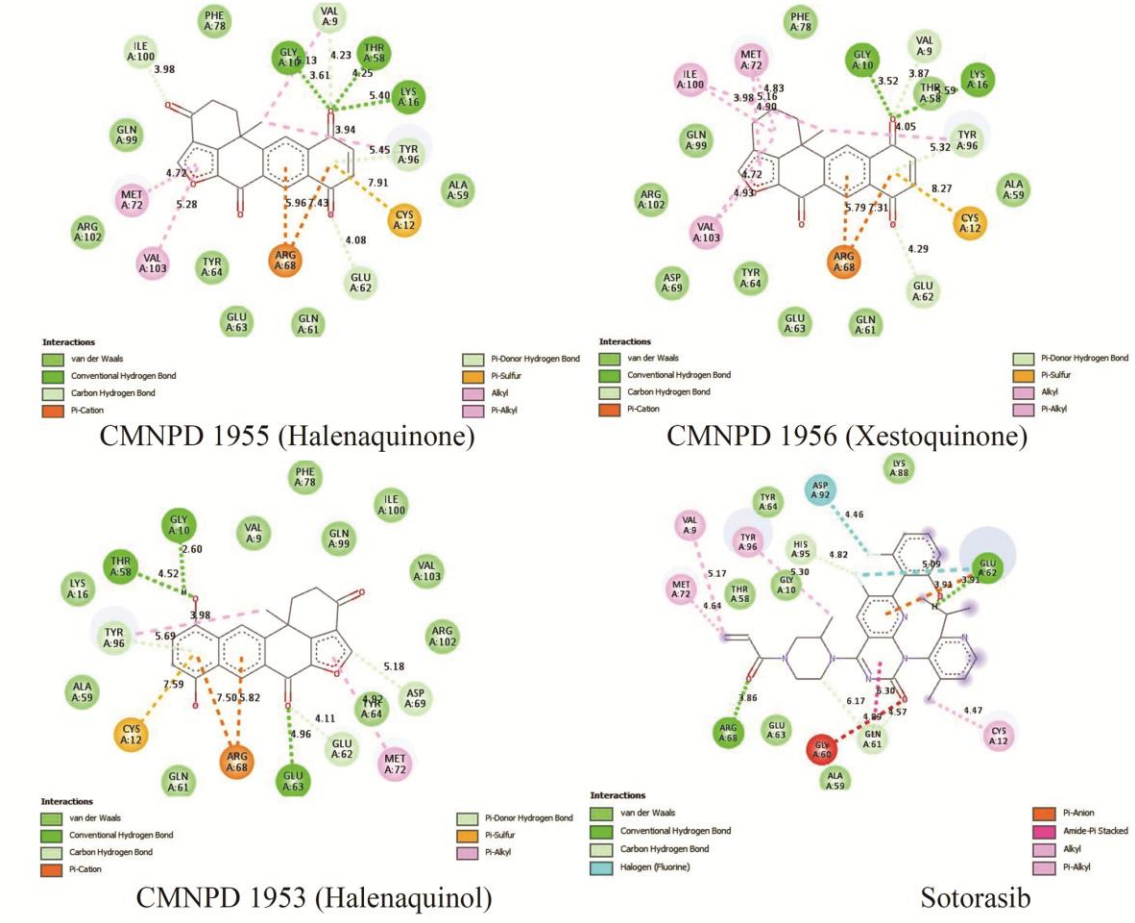


Fig. 1 — Molecular docking interactions data of CMNPD 1955 (Halenaquinone), CMNPD 1956 (Xestoquinone), CMNPD 1953 (Halenaquinol), and Sotorasib with KRAS G12C receptor.

MET 72 (3.98 Å), VAL 103 (6.85 Å) by (Pi-Alkyl interaction); and VAL 9, LYS 16, THR 58, SER 65, GLN 61, ILE 100, (van der waals interactions). Complexed 7L8 interacted with KRAS G12D receptor *via* GLY 10 (4.42 Å), TYR 64 (4.57 Å), ARG 68 (5.23 Å), HIS 95 (5.06 Å) by (hydrogen bond interaction); ARG 102 (8.01 Å) (Pi-Cation interaction); VAL 103 (6.57 Å) by (Pi-Alkyl interaction); TYR 96 (5.34 Å) (Pi-Pi interaction); and VAL 9, LYS 16, THR 58, SER 65, GLN 61, ILE 100, (van der waals interactions) (Fig. 2). The common interacting residues between complexed ligand, best docked molecules and standard MRTX 1133 confirmed that molecules were effectively docked within the receptor active site [50].

## MD Simulation Data

In case of KRASG12C inhibition: KRASG12C apoenzyme, CMNPD 1955 (Halenaquinone) - KRASG12C complex, CMNPD 1956 (Xestoquinone) – KRASG12C complex, CMNPD 1953 (Halenaquinol) – KRASG12C complex, and Sotorasib – KRASG12C complex were considered for MD simulation studies. Average RMSD value of KRASG12C apoprotein was 1.76 Å. RMSF data of KRASG12C apoprotein showed that maximum fluctuation showed below 2.63 Å. Average radius of gyration and SASA values of KRASG12C apoprotein were 1.21 nm and 92.06 $nm^2$, respectively. Average RMSD values of CMNPD 1955 (Halenaquinone)–KRASG12C complex, CMNPD 1956 (Xestoquinone)– KRASG12C complex, CMNPD 1953 (Halenaquinol)– KRASG12C complex, and Sotorasib – KRASG12C complex were 1.26 Å, 1.69 Å, 1.27 Å, and 1.99 Å, respectively. RMSD values of CMNPD 1955, CMNPD 1953, and sotorasib showed maximum stability throughout simulation. KRAS G12C apoenzyme and CMNPD 1956 showed fluctuations during simulation (Fig. 3A). Among the

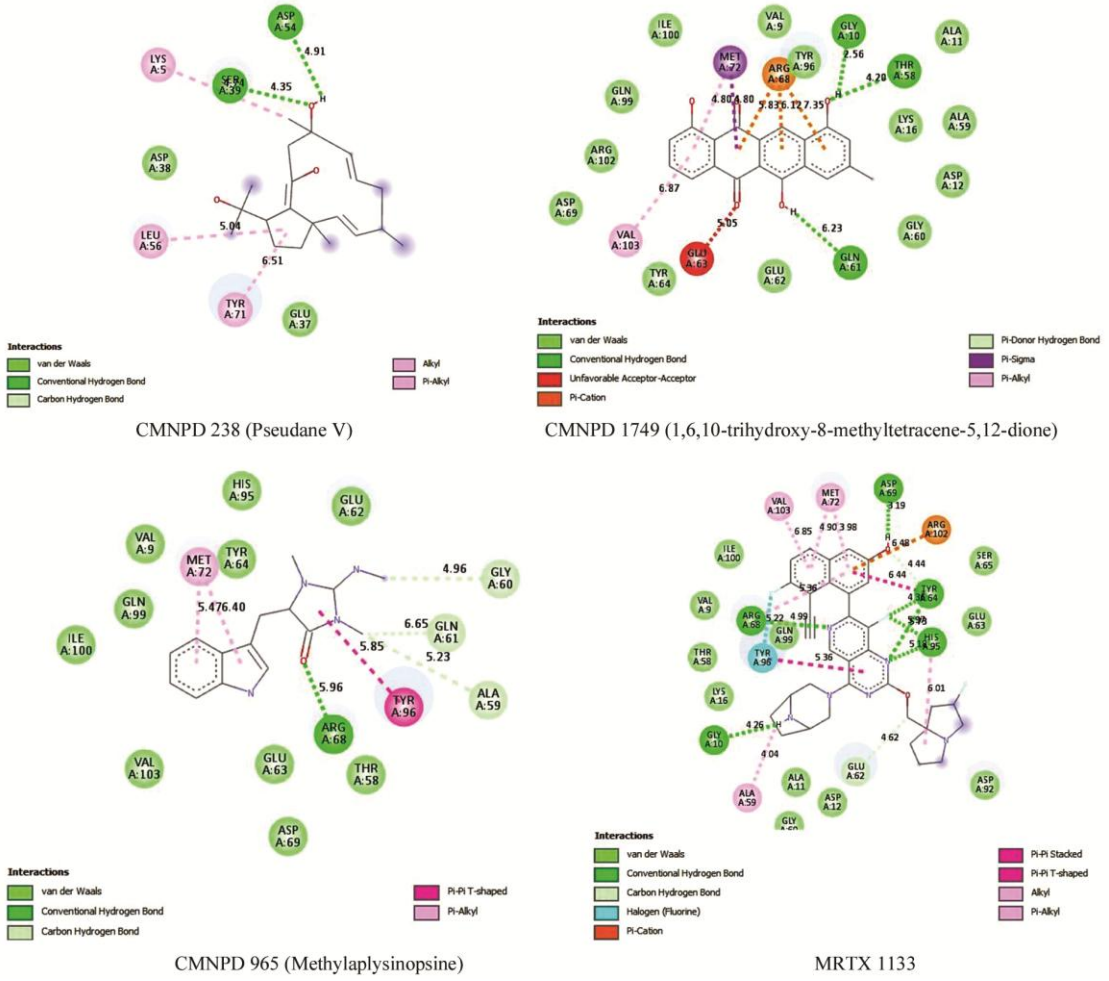


Fig. 2 — Molecular docking interactions data of CMNPD 238 (Pseudane V), CMNPD 1749 (1,6,10-trihydroxy-8-methyltetracene-5, 12-dione), CMNPD 965 (Methylaplysinopsine), and MRTX 1133 with KRAS G12D receptor.

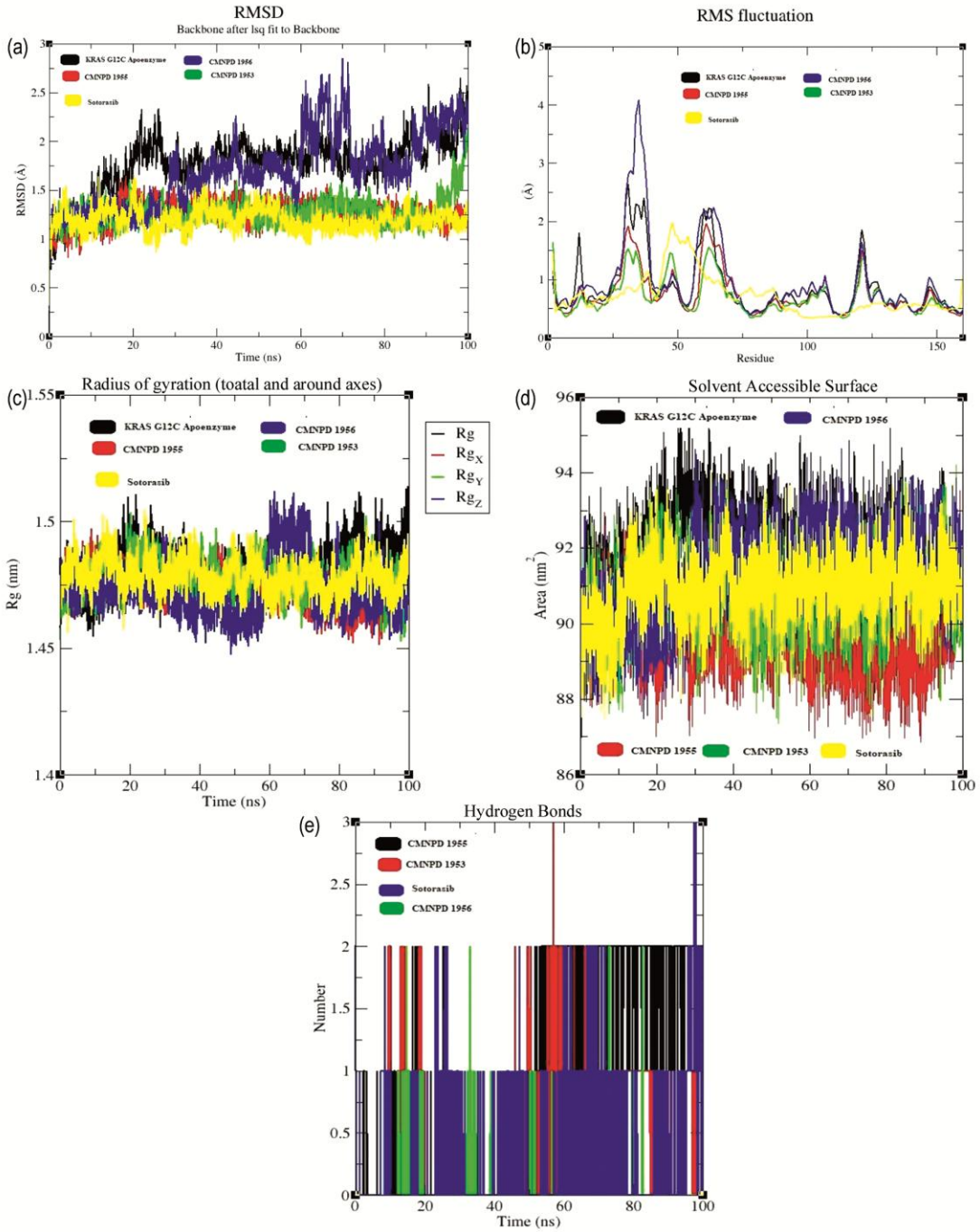


Fig. 3 — (A-E) MD Simulation data of CMNPD 1955 (Halenaquinone), CMNPD 1956 (Xestoquinone), CMNPD 1953 (Halenaquinol), and Sotorasib with KRAS G12C receptor.

selected marine drugs CMNPD 1955, CMNPD 1953, and standard sotorasib confirmed that all the ligands attained a stable configuration within the receptor during interactions. RMSF diagram showed that in most of simulation run fluctuations were limited with 2.8 Å except CMNPD 1956 (Xestoquinone). In case of KRASG12C apoenzyme, CMNPD 1955 (Halenaquinone)–KRASG12C complex, CMNPD 1956 (Xestoquinone)–KRASG12C complex, CMNPD 1953 (Halenaquinol)–KRASG12C complex, and Sotorasib–KRASG12C complex RMSF values were fluctuated from (0.39-2.63) Å, (0.33-2.855) Å, (0.38-4.086) Å, (0.37-1.92) Å, and (0.32-2.47) Å, respectively (Fig. 3B). PRO 34, THR 35, ILE 36, and

GLU 37 showed maximum fluctuations during simulation because these residues were not present during the interactions[51]. The average radius of gyration values of CMNPD 1955 (Halenaquinone), CMNPD 1956 (Xestoquinone), CMNPD 1953 (Halenaquinol), and Sotorasib complexed with KRASG12C receptor were 1.20 nm, 1.18 nm, 1.19 nm, and 1.20 nm, respectively[52]. CMNPD 1956 (Xestoquinone) showed some fluctuation in radius of gyration value but near 70 ns it reached a lower value (Fig. 3C). Here, the continuous decreasing radius of gyration values is associated with good stability. The average SASA values of CMNPD 1955 (Halenaquinone), CMNPD 1956 (Xestoquinone), CMNPD 1953 (Halenaquinol), and Sotorasib complexed with KRASG12C receptor were 89.70 $nm^2$, 91.28 $nm^2$, 91.20 $nm^2$, and 90.90 $nm^2$, respectively. SASA values displayed that all complexes attained stable structures during simulation (Fig. 3D). Hydrogen bond analysis of CMNPD 1955 (Halenaquinone), CMNPD 1956 (Xestoquinone), CMNPD 1953 (Halenaquinol), and Sotorasib complexed with KRASG12C receptor showed interactive hydrogen bond (10-20, 50-100) ns, and (0-100) ns, respectively (Fig. 3E). In case of KRASG12D inhibition: KRASG12D apoenzyme, CMNPD 238 (Pseudane V) –KRASG12D complex, CMNPD 1749 (1,6,10-trihydroxy-8-methyltetracene-5,12-dione) -KRASG12D complex, CMNPD 965 (Methylaplysinopsine) -KRASG12D complex, and MRTX 1133 - KRASG12D complex were considered for MD simulation studies. Average RMSD value of KRASG12D apoprotein was 1.82 Å. RMSF data of KRASG12D apoprotein showed that maximum fluctuation showed below 3.3 Å. Average radius of gyration and SASA values of KRASG12D apoprotein were 1.19 nm and 92.95 $nm^2$, respectively. Average RMSD values of CMNPD 238 (Pseudane V) -KRASG12D complex, CMNPD 1749 (1,6,10-trihydroxy-8-methyltetracene-5,12-dione) -KRASG12D complex, CMNPD 965 (Methylaplysinopsine) -KRASG12D complex, and MRTX 1133 - KRASG12D complex were 1.91 Å, 1.44 Å, 1.45 Å, and 1.82 Å, respectively. RMSD value of CMNPD 238 show a sudden increase during (30-90) ns and then stabilize. RMSD values of KRAS G12D apoenzyme, CMNPD 1749 and CMNPD 965 almost stable version during the simulation (Fig. 4A).

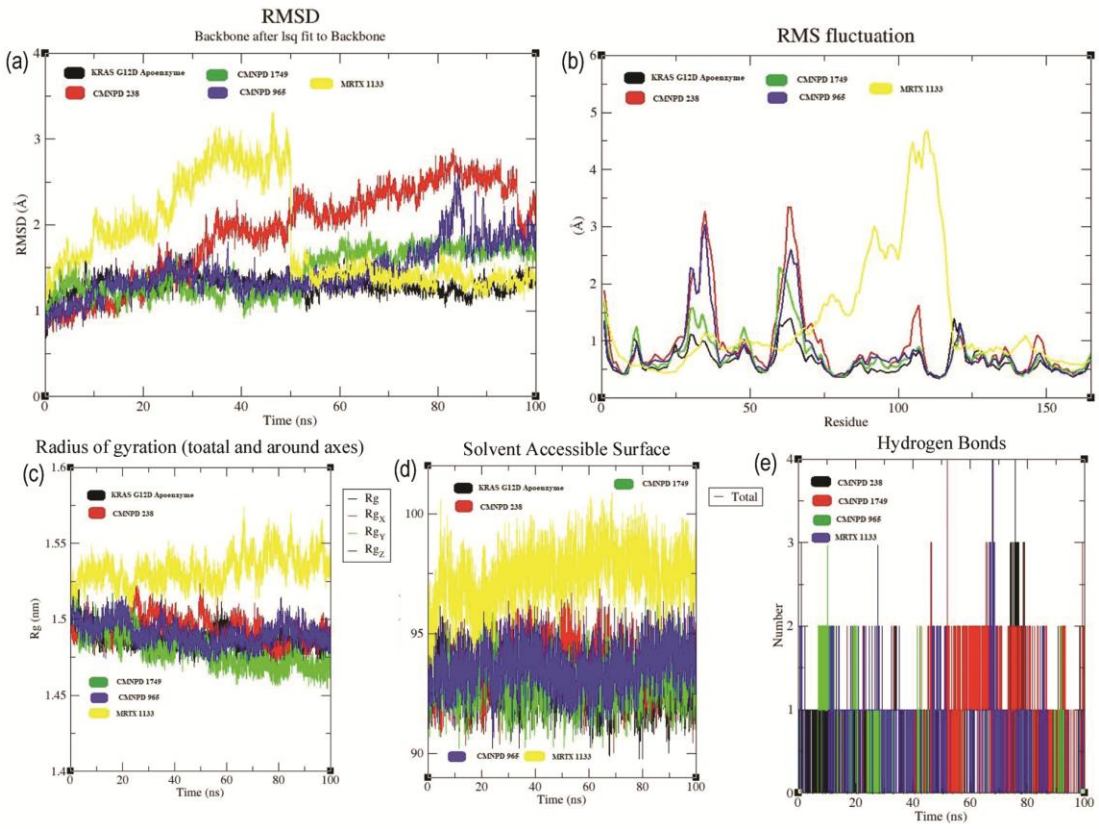


Fig. 4 — (A-E) MD Simulation data of CMNPD 238, CMNPD 1749, CMNPD 965, and MRTX 1133 with KRASG12D receptor

RMSD value of MRTX 1133 showed an increment between (0-50) ns, and stabilized between (50-100) ns. RMSF diagram of KRASG12D apoenzyme, CMNPD 238 (Pseudane V) -KRASG12D complex, CMNPD 1749 (1,6,10-trihydroxy-8-methyltetracene-5,12-dione) -KRASG12D complex, and CMNPD 965 (Methylaplysinopsine)-KRASG12D complex showed maximum fluctuation up to 3.3 Å, and standard MRTX 1133 observed with more than 4.5 Å. In case of KRASG12D apoenzyme, CMNPD 238 (Pseudane V)-KRASG12D complex, CMNPD 1749 (1,6,10-trihydroxy-8-methyltetracene-5,12-dione)-KRASG12D complex, CMNPD 965 (Methylaplysinopsine)-KRASG12D complex, and MRTX 1133-KRASG12D complex RMSF values were fluctuated from (0.33-1.394) Å, (0.35-3.339) Å, (0.34-2.29) Å, (0.36-3.037) Å, and (0.43-4.676) Å, respectively. THR 35, and TYR 64 showed maximum fluctuations during simulation because these residues were not directly interacted with receptor[53] (Fig. 4B). The average radius of gyration values of CMNPD 238 (Pseudane V), CMNPD 1749 (1,6,10-trihydroxy-8-methyltetracene-5,12-dione), CMNPD 965 (Methylaplysinopsine), and MRTX 1133 complexed with KRASG12D receptor were 1.22 nm, 1.21 nm, 1.23 nm, and 1.26 nm, respectively. MRTX 1133 showed higher radius of gyration value than other molecules. Here, the continuous decreasing radius of gyration values associated with good stability (Fig. 4C). The average SASA values of CMNPD 238 (Pseudane V), CMNPD 1749 (1,6,10-trihydroxy-8-methyltetracene-5,12-dione), CMNPD 965 (Methylaplysinopsine), and MRTX 1133 complexed with KRASG12D receptor were 93.62 $nm^2$, 93.04 $nm^2$, 93.62 $nm^2$, and 97.42 $nm^2$, respectively. SASA values displayed that all complexes attained a stable-structures during simulation (Fig. 4D)[54]. Hydrogen bond analysis of CMNPD 238 (Pseudane V), CMNPD 1749 (1,6,10-trihydroxy-8-methyltetracene-5,12-dione), CMNPD 965 (Methylaplysinopsine), and MRTX 1133 complexed with KRASG12D receptor showed interactive hydrogen bonds throughout the simulation (Fig. 4E).

## MMPBSA Analysis Data

MMPBSA analysis data showed that binding energies of CMNPD 1955 (Halenaquinone), CMNPD 1956 (Xestoquinone), CMNPD 1953 (Halenaquinol), Sotorasib interacted with KRAS G12C receptor were –16.132 kJ/mol, –15.211 kJ/mol, –3.953 kJ/mol, and −3.463 kJ/mol, respectively[55]. Van der Waal, Electrostatic, Polar solvation, and SASA energies were positively contributed in binding energies of CMNPD 1955 (Halenaquinone), and CMNPD 1956 (Xestoquinone), respectively. van der Waal, electrostatic, and SASA energies were positively and polar salvation energies were negatively impacted in binding energies of CMNPD 1953 (Halenaquinol), and sotorasib (Table S4). MMPBSA analysis data showed that binding energies of CMNPD 238 (Pseudane V), CMNPD 1749 (1,6,10-trihydroxy-8-methyltetracene-5,12-dione), CMNPD 965 (Methylaplysinopsine), and MRTX 1133 with KRAS G12D receptor were –4.903 kJ/mol, –2.794 kJ/mol, –2.862 kJ/mol, and –2.894 kJ/mol, respectively. In all complexes van der waal, electrostatic, SASA energies were positively, and polar solvation energies were negatively contributed in binding energies (Table S5) [56].

## DFT Analyses Data

### Frontier Molecular Orbital Analysis data

Frontier Molecular Orbital Analysis data of CMNPD 1955 (Halenaquinone), CMNPD 1956 (Xestoquinone), CMNPD 1953 (Halenaquinol), sotorasib, CMNPD 238 (Pseudane V), CMNPD 1749 (1,6,10-trihydroxy-8-methyltetracene-5,12-dione), CMNPD 965 (Methylaplysinopsine), MRTX 1133 have HOMO and LUMO orbital energies (eV) of –7.42, –6.88, –5.74, –6.34, –6.25, –6.09, –5.08, –5.66 and –3.72, –3.53, –2.34, –2.74, –1.52, –3.23, –1.49, –2.17, respectively[57]. The HOMO and LUMO orbitals' energy gap reveals the molecules' chemical strength and reactivity. HOMO and LUMO energy gaps of CMNPD 1955 (Halenaquinone), CMNPD 1956 (Xestoquinone), CMNPD 1953 (Halenaquinol), sotorasib, CMNPD 238 (Pseudane V), CMNPD 1749 (1,6,10-trihydroxy-8-methyltetracene-5,12-dione), CMNPD 965 (Methylaplysinopsine), and MRTX 1133 were 3.70, 3.35, 3.40, 3.60, 4.73, 2.86, 3.59, and 3.49, respectively. Table 1 included the values for the energy gap (ΔE) between the HOMO and LUMO, softness, electronegativity, chemical hardness, and electrophilicity index. Among the selected marine drugs effective against KRAS G12C and KRAS G12D, CMNPD 1956 (Xestoquinone) and CMNPD 1749 (1,6,10-trihydroxy-8-methyltetracene-5,12-dione) referred as soft molecule and because of the lesser energy gap system. The more excellent value of the electrophilicity index designated, the higher the chemical reactivity[58]. CMNPD 1955 (Halenaquinone) and CMNPD 1749 (1,6,10-

Table 1 — FMO analysis data of CMNPD 1955 (Halenaquinone), CMNPD 1956 (Xestoquinone), CMNPD 1953 (Halenaquinol), Sotorasib, CMNPD 238 (Pseudane V), CMNPD 1749 (1,6,10-trihydroxy-8-methyltetracene-5,12-dione), CMNPD 965 (Methylaplysinopsine), and MRTX 1133.

| S N | Molecule Name | $E_{HOMO}$ (eV) | $E_{LUMO}$ (eV) | ΔE gap (eV) | I | A | η | ζ | μ | Ψ |
|---|---|---|---|---|---|---|---|---|---|---|
| 1. | CMNPD 1955 (Halenaquinone)* | –7.42 | –3.72 | 3.70 | 7.42 | 3.72 | 1.65 | 0.27 | 5.57 | 8.38 |
| 2. | CMNPD 1956(Xestoquinone)* | –6.88 | –3.53 | 3.35 | 6.88 | 3.53 | 1.67 | 0.29 | 5.20 | 8.07 |
| 3. | CMNPD 1953 (Halenaquinol)* | –5.74 | –2.34 | 3.40 | 5.74 | 2.34 | 1.70 | 0.29 | 4.04 | 4.80 |
| 4. | Sotorasib* | –6.34 | –2.74 | 3.60 | 6.34 | 2.74 | 1.8 | 0.27 | 4.54 | 5.72 |
| 5. | CMNPD 238 (Pseudane V)# | –6.25 | –1.52 | 4.73 | 6.25 | 1.52 | 2.37 | 0.21 | 3.88 | 3.18 |
| 6. | CMNPD 1749 (1,6,10-trihydroxy-8-methyltetracene-5,12-dione)# | –6.09 | –3.23 | 2.86 | 6.09 | 3.23 | 1.43 | 0.34 | 4.66 | 7.59 |
| 7. | CMNPD 965 (Methylaplysinopsine) # | –5.08 | –1.49 | 3.59 | 5.08 | 1.49 | 1.79 | 0.27 | 3.62 | 3.65 |
| 8. | MRTX 1133# | –5.66 | –2.17 | 3.49 | 5.66 | 2.17 | 1.74 | 0.28 | 3.91 | 4.39 |

* = KRAS G12C # = KRAS G12D

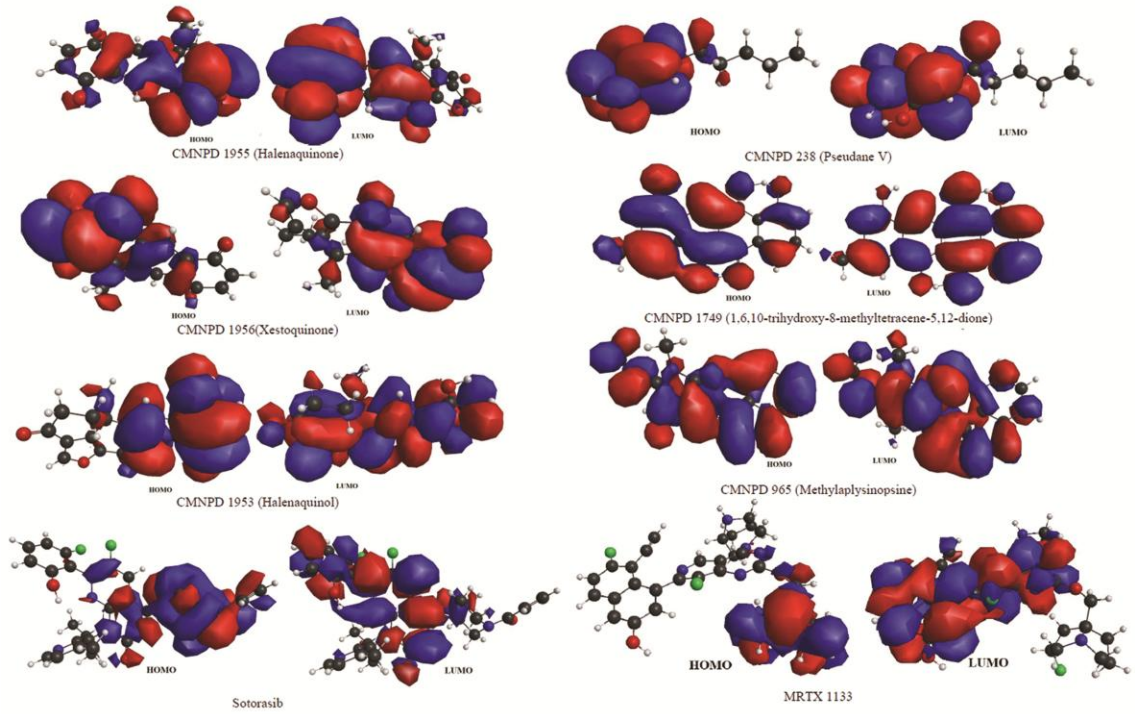


Fig. 5 — FMO analysis data of CMNPD 1955 (Halenaquinone), CMNPD 1956 (Xestoquinone), CMNPD 1953 (Halenaquinol), Sotorasib, CMNPD 238 (Pseudane V), CMNPD 1749 (1,6,10-trihydroxy-8-methyltetracene-5,12-dione), CMNPD 965 (Methylaplysinopsine), MRTX 1133.

trihydroxy-8-methyltetracene-5,12-dione) showed maximum electrophilicity (Fig. 5)[59].

## Molecular Electrostatic Potential data

Cyclohex-2-ene-1,4-dione and (5aS)-5a,6,7-trimethyl-1,3,4,5,5a,8-hexahydroacenaphthylene groups are preferred zones of electrophilic and nucleophilic attacks for CMNPD 1955 (Halenaquinone), and CMNPD 1956 (Xestoquinone). Cyclohex-2-ene-1,4-diol, and (5aS)-5a,6,7-trimethyl-1,3,4,5,5a,8-hexa hydroacenaphthylene groups are preferred zones of electrophilic and nucleophilic attacks for CMNPD 1953 (Halenaquinol)[60,61]. In sotorasib, the maximum molecule was covered with a blue-colored nucleophilic attack region, and a red electrophilic attack region was observed with cyano-piperazine, N =C-N-C-C= N groups and terminal ketone groups of 4-(4-acryloyl-2-methylpiperazin-1-yl)-6-fluoro-7- (2-fluoro-6-hydroxyphenyl)-1-(2-isopropyl-4-methylpyridin-3-yl) pyrido[2,3-d] pyrimidin-2(1H)-one[62]. In case of CMNPD 238 (Pseudane V) nitrogen atom and hydroxyl group responsible for electrophilic attack, and C=C group of phenyl ring responsible for nucleophilic attack. In

case of CMNPD 1749 (1,6,10-trihydroxy-8-methyltetracene-5,12-dione): ketone and hydroxyl groups responsible for electrophilic attack and rest of the molecule 8-methyl-5,12-dihydrotetracene group is electrically neutral[63]. In case of CMNPD 965 (Methylaplysinopsine): structure is divided into two equal electrophilic and nucleophilic attacks. 2-fluorohexahydro-1H-pyrrolizine, 5,6-dimethyli dene cyclo hexa-1,3-diene and F-C = C-N = C-O groups of 4-(4-(3-(3,8-diaza bicyclo[3.2.1]octan-3-yl)-8-fluoro-2-((2- fluorohexahydro-1H-pyrrolizin-7a- yl) methoxy) pyrido[4,3-d] pyrimidin-7-yl)-5-ethynyl-6-fluoronaphthalen-2-ol responsible for nucleophilic and electrophilic attacks in case of MRTX 1133 (Fig. 6) [64,65].

**PCA and FEL Analysis data**

PCA is used to identify the complexity of ligand-receptor complex obtained from MD simulation analysis is principal component analysis by modifying transitional and rotational movements within the trajectory[66,67]. The dynamics of complex structure was based on two dimensional projections of trajectories on eigenvectors 1 and 2. PCA is also associated with atomic movement and motion dynamics[68]. The eigenvector values of KRAS G12C apoprotein, KRASG12C-CMNPD 1955, KRASG12C-CMNPD1956, KRASG12C-CMNPD1953, and KRAS G12D apoprotein, KRASG12D-CMNPD238, KRASG12D-CMNPD1749, and KRASG12D-CMNPD965 were determined. The essential subspace of KRAS G12C apoprotein and KRAS G12D apoprotein of eigenvector 1 were in the range from (4.0 to –3.0) nm, *vs*. eigenvector 2 in the range from (–3.0 to 2.0) nm, and from (2.0 to –3.0) nm, *vs*. eigenvector 2 in the range from (–2.0 to 2.0) nm, respectively present in the larger cluster for apoprotein[69]. In case of KRASG12C-CMNPD 1955, KRASG12C-CMNPD1956, KRASG12C-CMNPD1953, 6AYC-abyssinone III, and KRASG12D-CMNPD238, KRASG12D-CMNPD1749, and KRASG12D-

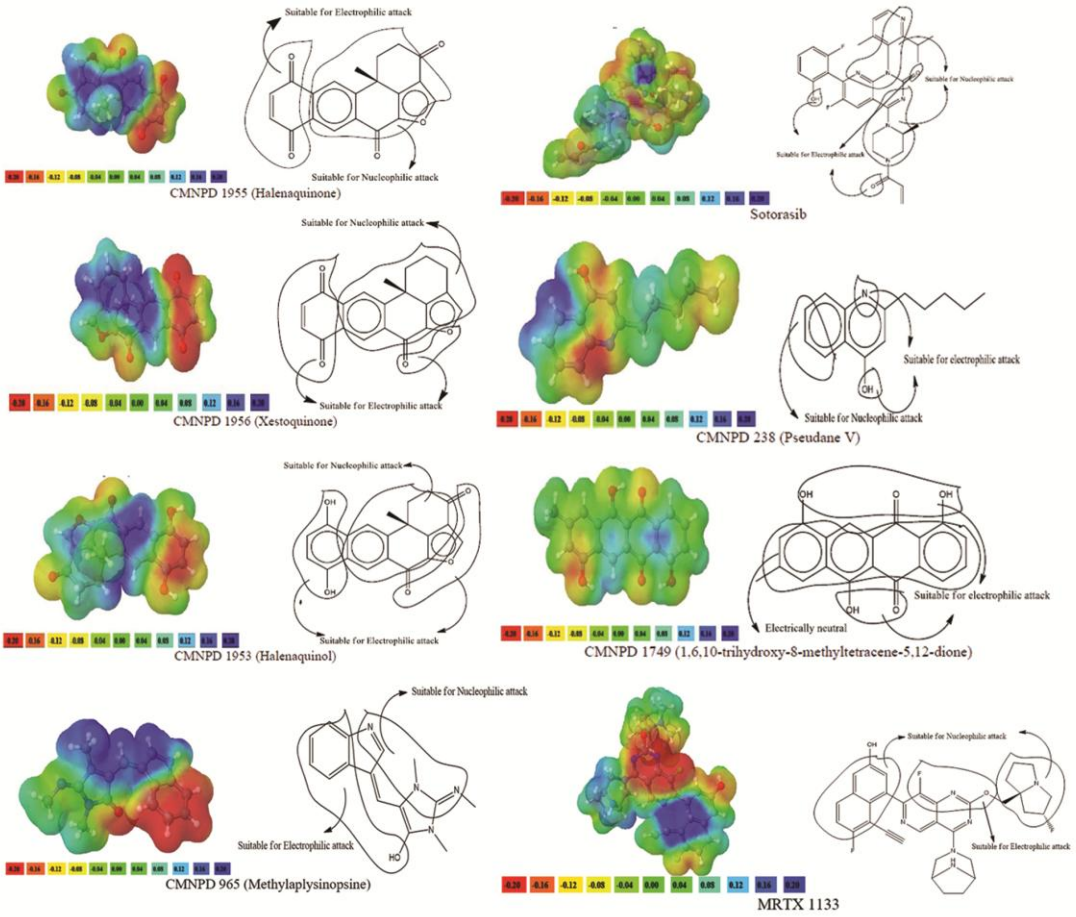


Fig. 6 — MEP analysis data of CMNPD 1955 (Halenaquinone), CMNPD 1956 (Xestoquinone), CMNPD 1953 (Halenaquinol), Sotorasib, CMNPD 238 (Pseudane V), CMNPD 1749 (1,6,10-trihydroxy-8-methyltetracene-5,12-dione), CMNPD 965 (Methylaplysinopsine), MRTX 1133.

CMNPD965, eigenvector 1 values of were (–2.0 to 3.0) nm, (–4.0 to 3.0) nm, (–3.0 to 3.0) nm, (–3.0 to 4.0) nm, (–2.0 to 3.0) nm, (–2.0 to 5.0) nm, *vs*. eigenvector 2 in the range from (–2.0 to 3.0) nm, (–4.0 to 3.0) nm, (–2.0 to 3.0) nm, (–3.0 to 2.0) nm, (–3.0 to 2.0) nm, (–2.0 to 3.0) nm, respectively[70]. These data confirmed the well defined internal motion observed with KRASG12C-CMNPD 1955, KRASG12C-CMNPD1956, KRASG12C-CMNPD 1953, and KRASG12D-CMNPD238, KRASG12D-CMNPD1749, and KRASG12D-CMNPD965 complexes (Fig. 7)[71]. Through PCA, we were able to identify the most likely and significant changes in protein conformation that occurred during ligand binding or complex formation in MD. The states of global energy minima are displayed in the Gibbs energy landscape (FEL)[72]. As per FEL blue/green contour reflects stable local global energy minima state, unfavorable state represented by yellow color, and high free energy landscape unstable conformational state associated with red region. The free energy landscape values of KRAS G12C apoprotein, KRASG12C-CMNPD 1955, KRASG 12C-CMNPD1956, KRASG12C-CMNPD1953, and KRAS G12D apoprotein, KRASG12D-CMNPD238, KRASG12D-CMNPD1749, and KRASG12D-CMNPD965 ranged from (0-12.5) kJ/mol, (0-10.7) kJ/mol, (0-14.4) kJ/mol, (0-11.6) kJ/mol, (0-11.5) kJ/mol, (0-10.4) kJ/mol, (0-11.6) kJ/mol, and (0-12.7) kJ/mol, respectively (Fig. 8)[73]. Most of the central

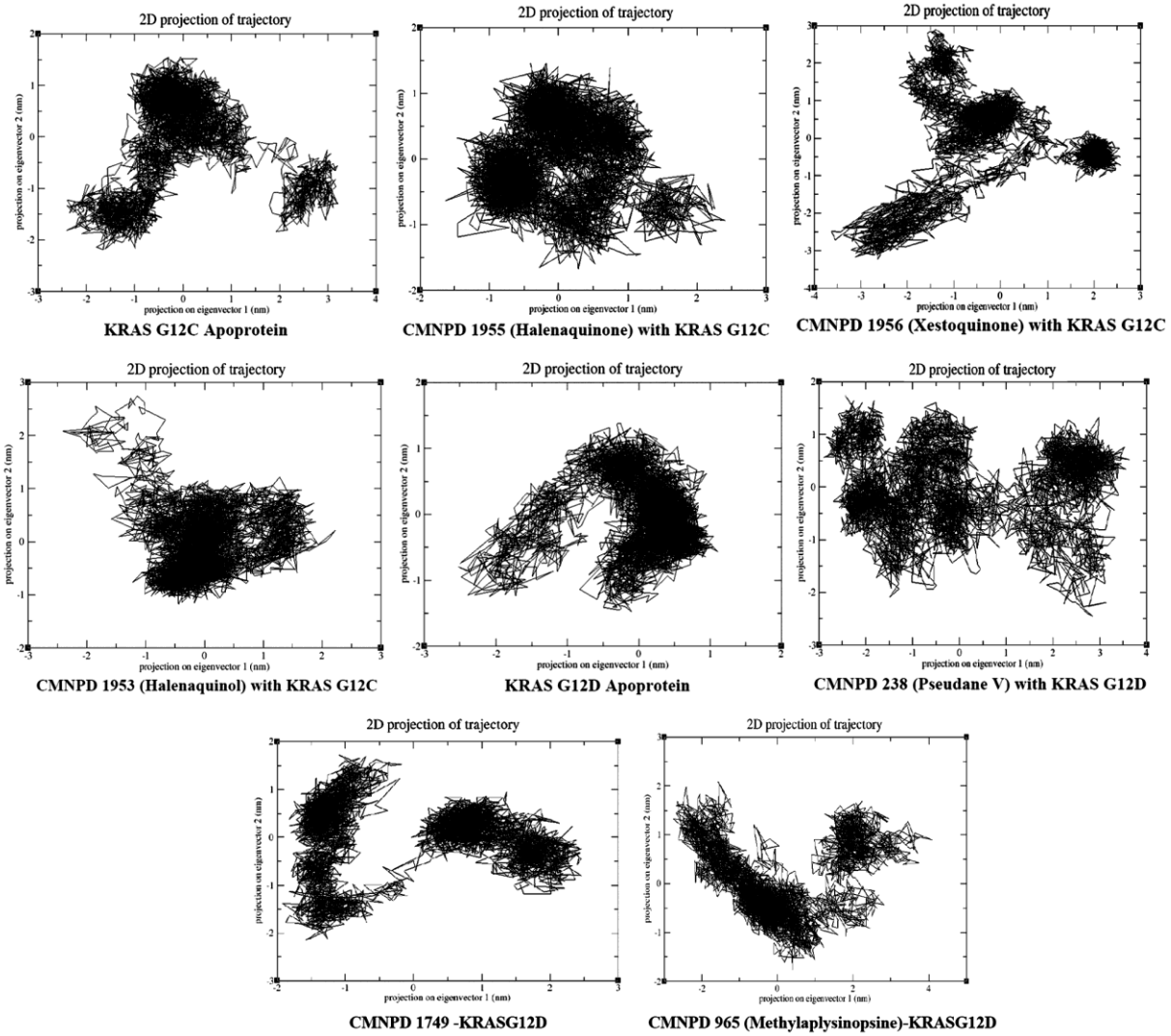


Fig. 7 — FEL analysis data of KRAS G12C apoprotein, KRASG12C-CMNPD 1955, KRASG12C-CMNPD1956, KRASG12C-CMNPD1953, KRAS G12D apoprotein, KRASG12D-CMNPD238(Pseudane V), KRASG12D-CMNPD1749(1,6,10-trihydroxy-8-methyltetracene-5,12-dione), and KRASG12D-CMNPD965(Methylaplysinopsine).

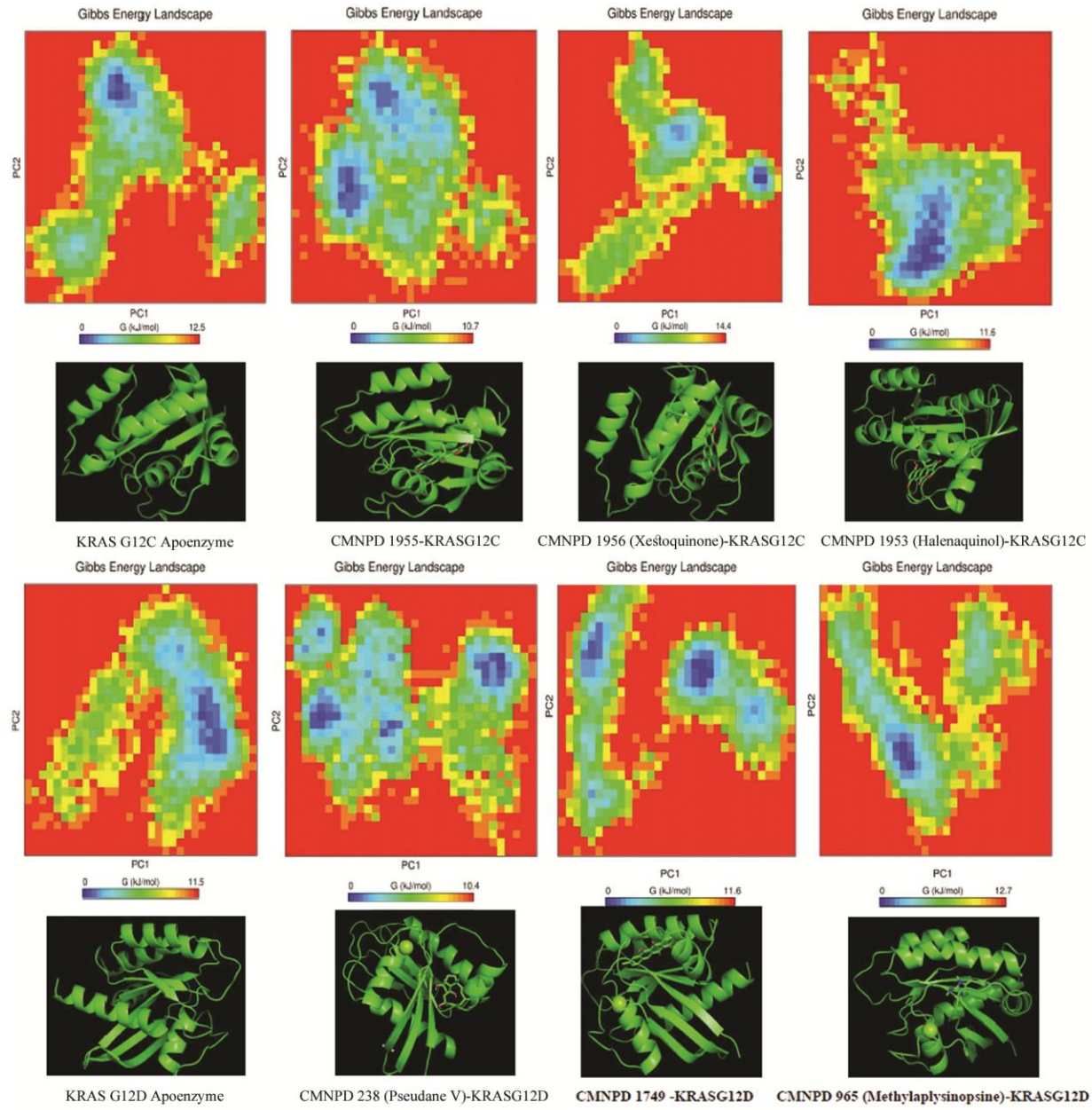


Fig. 8 — FEL analysis data of KRAS G12C apoprotein, KRASG12C-CMNPD 1955, KRASG12C-CMNPD1956, KRASG12C-CMNPD1953, KRAS G12D apoprotein, KRASG12D-CMNPD238(Pseudane V), KRASG12D-CMNPD1749(1,6,10-trihydroxy-8-methyltetracene-5,12-dione), and KRASG12D-CMNPD965(Methylaplysinopsine).

contour regions comprised of blue-green regions represents stable conformation of receptor and in some instances mixed with central blue-green regions tinted with yellow region reflects slightly stable but not unstable ligand-receptor conformation[74,75].

## ADMET Analysis data

Pharmacokinetic behavior analyses of 1699 marine based compounds were performed using Swiss ADME web portal (http://www.swissadme.ch/) accessed within (10.09.2024-17.09.2024). In this analysis, molecules were subjected to *in silico* oral solubility (Log S), partition coefficient (Log P), blood brain barrier permeability, and cytochrome P450 microsomal enzyme inhibitor profiling[76]. Molecules with solubility parameter (Log S) value within –4 to +0.5 were considered as good aqueous solubility. Out of 1699 molecules 1052 molecules showed less probability to become soluble in aqueous environment. Molecules with a partition coefficient

(Log P) value less than 3.0 are considered for good permeation of biological membranes. Only 540 molecules showed good Log P value with greater probability to permeate a biological membrane[77,78]. Blood brain barrier permeability confirmed the molecules with higher probability to cross the membrane and reach brain[79,80]. Among the 1699 molecules 1014 molecules showed higher probability to cross blood brain barrier. Also, among the selected marine based compounds 330, 696, 868, 330, and 397 molecules were CYP 1A2, 2C19, 2C9, 2D6, and 3A4 inhibitors, respectively[81,82]. All microsomal enzymes were participated in Phase I biotransformation, so these mentioned molecules were either directly participated in Phase II biotransformation or there is a scope of change in the formulation phase (Table S6). All molecules showed good probability as non-mutagenic, non-tumorigenic, non-irritant, and non-reproductive toxicant (Table S7) [83,84].

## Conclusion

After exhaustive computational research, we identified that, Halenaquinone, Xestoquinone, Halenaquinol, and Pseudane V, 1,6,10-trihydroxy-8-methyltetracene-5,12-dione, methylaplysinopsine showed maximum binding potentials against KRAS G12C and G12D, respectively. These findings open a new door for researchers to pharmacologically establish the potential of the molecules.

## Supplementary Information

Table S1: List of Marine drugs with Smiles and Biological source; Table S2. Molecular docking interaction data of selected marine drugs with KRAS G12C receptor; Table S3. Molecular docking interaction data of selected marine drugs with KRAS G12D receptor;Table S4. MMPBSA Data of CMNPD 1955 (Halenaquinone), CMNPD 1956 (Xestoquinone), CMNPD 1953 (Halenaquinol), Sotorasib interacted with KRAS G12C receptor; Table S5. MMPBSA Data of CMNPD 238 (Pseudane V), CMNPD 1749 (1,6,10-trihydroxy-8-methyltetracene-5,12-dione), CMNPD 965 (Methylaplysinopsine), and MRTX 1133 with KRAS G12D receptor; Table S6 *In silico* Pharmacokinetic behavior analysis data of Selected Marine based Compounds; Table S7 *In silico* toxicity prediction data of Selected Marine based Compounds; Fig. S1 Surrounding residues of complexed ligands LXD and 7L8 with 8AFB (KRAS G12C) and 7RT1 (KRAS G12D) receptors; Fig. S2 Protein structural feature of 8AFB (KRAS G12C) receptor; Fig. S3 Protein structural feature of 7RT1 (KRAS G12D) receptor.

## Acknowledgement

This study is supported by Division of Research & Innovation, Uttaranchal University, Dehradun, India to Supriyo Saha under the seed money grant reference no UU/DRI/SM/2024-25/018.

## Supplementary Information

Supplementary information is available in the website http://nopr.niscpr.res.in/handle/123456789/58776.

## References

1 Luo J, *Seminar Onco*, 48 (2021) 10.
2 Huang L, Guo Z, Wang F, & Fu L, *Sig Trans Targeted Therap*, 6 (2021) 386.
3 Hofmann M H, Gerlach D, Misale S, Petronczki M & Kraut N, *Cancer Discov*, 12 (2022) 924.
4 Stickler S, Rath B & Hamilton G, *Onco Res Feat Pre Clin Cancer Therap*, 32 (2024) 799.
5 Negri F, Bottarelli L, De A G L & Gnetti L, *Int J Mol Sci*, 23 (2022) 4120.
6 Bannoura S F, Uddin M H, Nagasaka M, Fazili F, Al-Hallak M N, Philip P A, El-Rayes B & Azmi A S, *Can Meta Rev*, 40 (2021) 819.
7 Canon J, Rex K, Saiki A Y, Mohr C, Cooke K, Bagal D, Gaida K, Holt T, Knutson C G, Koppada N, Lanman B A, Werner J, Rapaport A S, Miguel T S, Ortiz R, Osgood T, Sun J, Zhu X, McCarter J D, Volak L P, Houk BE, Fakih M G, O'Neil BH, Price T J, Falchook G S, Desai J, Kuo J, Govindan R, Hong D S, Ouyang W, Henary H, Arvedson T, Cee V J & Lipford J R, *Nature*, 575 (2019) 217.
8 Bekaii S T S, Yaeger R, Spira A I, Pelster M S, Sabari J K, Hafez N, Barve M, Velastegui K, Yan X, Shetty A, Der T H & Pant S, *J Clin Oncology*, 41(2023) 4097.
9 Lim T K H, Skoulidis F, Kerr K M, Ahn M, Kapp J R, Soares F A & Yatabe Y, *Lung Cancer*, 184 (2023) 107293.
10 De L A J, Johnson M L, Mazieres J, Dingemans A C, Mountzios G, Pless M, Wolf J, Schuler M, Lena H, Skoulidis F, Yoneshima Y, Kim S, Linardou H, Novello S, Van Der Wekken A J, Chen Y, Peters S, Felip E, Solomon B J, Ramalingam S S, Dooms C, Lindsay C R, Ferreira C G, Blais N, Obiozor C C, Wang Y, Mehta B, Varrieur T, Ngarmchamnanrith G, Stollenwerk B, Waterhouse D & Paz A L, *Lancet*, 401 (2023) 733.
11 Skoulidis F, Li B T, Dy G K, Price T J, Falchook G S, Wolf J, Italiano A, Schuler M, Borghaei H, Barlesi F, Kato T, Curioni F A, Sacher A, Spira A, Ramalingam S S, Takahashi T, Besse B, Anderson A, Ang A, Tran Q, Mather O, Henary H, Ngarmchamnanrith G, Friberg G, Velcheti V & Govindan R, *New Eng J Med*, 384 (2021) 2371.
12 Nakajima E C, Drezner N Li X, Mishra K P S, Liu Y, Zhao H, Bi Y, Liu J, Rahman A, Wearne E, Ojofeitimi I, Hotaki L T, Spillman D, Pazdur R, Beaver J A & Singh H, *Clin Can Res*, 28 (2021) 1482.
13 Wang X, Allen S, Blake J F, Bowcut V, Briere D M, Calinisan A, Dahlke J R, Fell J B, Fischer J P, Gunn R J,

Hallin J, Laguer J, Lawson J D, Medwid J, Newhouse B, Nguyen P, O'L J M, Olson P, Pajk S, Rahbaek L, Rodriguez M, Smith C R, Tang T P, Thomas N C, Vanderpool D, Vigers G P, Christensen J G & Marx M A, *J Med Chem*, 65 (2021) 3123.

14 Hallin J, Bowcut V, Calinisan A, Briere D M, Hargis L, Engstrom L D, Laguer J, Medwid J, Vanderpool D, Lifset E, Trinh D, Hoffman N, Wang X, Lawson J D, Gunn R J, Smith C R, Thomas N C, Martinson M, Bergstrom A, Sullivan F, Bouhana K, Winski S, He L, Fernandez B J, Pavlicek A, Haling J R, Rahbaek L, Marx M A, Olson P & Christ J G, *Nat Med*, 28 (2022) 2171.

15 Liu C, Zheng S, Wang Z, Wang S, Wang X, Yang L, Xu H, Cao Z, Feng X, Xue Q, Wang Y, Sun N & He J, *Can Comm*, 42 (2022) 828.

16 Feng J, Hu Z, Xia X, Liu X, Lian Z, Wang H, Wang L, Wang C, Zhang X & Pang X, *Oncogene*, 42 (2023) 1620.

17 Zhou C, Li C, Luo L, Li X, Jia K, He N, Mao S, Wang W, Shao C, Liu X, Huang K, Yu Y, Cai X, Chen Y, Dai Z, Li W, Yu J, Li J, Shen F, Wang Z, He F, Sun X, Mao R, Shi W, Zhang J, Jiang T, Zhang Z, Li F & Ren S, *Cancer Cell*, 42 (2024) 1286.

18 Lentsch E, Li L, Pfeffer S, Ekici A B, Taher L, Pilarsky C & Grützmann R, *Int J Mol Sci*, 20 (2019) 5706.

19 Kataoka M, Kitazawa M, Nakamura S, Koyama M, Yamamoto Y, Miyazaki S, Hondo N, Tanaka H & Soejima Y, *Antican Res*, 43 (2023) 4341.

20 Lin Y, Pu S, Wang J, Wan Y, Wu Z, Guo Y, Feng W, Ying Y, Ma S, Meng X J, Wang W, Liu L, Xia Q & Yang X, *Gut*, 73 (2024) 1831.

21 Wu L, Ye K, Jiang S & Zhou G, *Marine Drug*, 19 (2021) 488.

22 Fernandes A S, Oliveira C, Reis R L, Martins A & Silva T H, *Marine Drug*, 20 (2022) 689.

23 Khalifa S A M, Elias N, Farag M A, Chen L, Saeed A, Hegazy M F, Moustafa M S, Abd El W A, Al-Mousawi S M, Musharraf S G, Chang F R, Iwasaki A, Suenaga K, Alajlani M, Göransson U & El-Seedi H R, *Marine Drug*, 17 (2019) 491.

24 Kortmansky J, & Schwartz G K, *Can Invest*, 21 (2003) 924.

25 Bajpai V K, Shukla S, Kang S M, Hwang S K, Song X, Huh Y S & Han Y K, *Marine Drug*, 16 (2018) 179.

26 Julianti E, Abrian I A, Wibowo M S, Azhari M, Tsurayya N, Izzati F, Juanssilfero A B, Bayu A, Rahmawati S I & Putra M Y, *Marine Drug*, 20 (2022) 67.

27 Fan M, Nath A K, Tang Y, Choi Y J, Debnath T, Choi E J & Kim E K, *Marine Drug*, 16 (2018) 160.

28 Newman D J & Cragg G M, *Marine Drug*, 12 (2014) 255.

29 Ha M W, Song B R, Chung H J & Paek S M, *Marine Drug*, 17 (2019) 500.

30 Guzmán E A, Peterson T A & Wright A E, *Marine Drug*, 21 (2023) 642.

31 Bröker J, Waterson A G, Smethurst C, Kessler D, Böttcher J, Mayer M, Gmaschitz G, Phan J, Little A, Abbott J R, Sun Q, Gmachl M, Rudolph D, Arnhof H, Rumpel K, Savarese F, Gerstberger T, Mischerikow N, Treu M, Herdeis L, Wunberg T, Gollner A, Weinstabl H, Mantoulidis A, Krämer O, McConnell D B & W Fesik S, *J Med Chem*, 65 (2022) 14614.

32 Wang X, Allen S, Blake J F, Bowcut V, Briere D M, Calinisan A, Dahlke J R, Fell J B, Fischer J P, Gunn R J, Hallin J, Laguer J, Lawson J D, Medwid J, Newhouse B, Nguyen P, O'L J M, Olson P, Pajk S, Rahbaek L, Rodriguez M, Smith C R, Tang T P, Thomas N C, Vanderpool D, Vigers G P, Christensen J G & Marx M A, *J Med Chem*, 65 (2022), 3123.

33 Park S W, Lee B H, Song S H & Kim M K, *J Struct Biol*, 215 (2023), 107939.

34 Kalman M & Ben-Tal N, *Bioinfo*, 26 (2010), 1299.

35 Olechnovič K & Venclovas Č, *Nucleic Acid Res*, 47 (2019), W437.

36 Goodsell D S, Sanner M F, Olson A J & Forli S, *Protein Sci*, 30 (2021), 31.

37 Quimque M T, Notarte K I, Adviento X A, Cabunoc M H, De Leon V N, Delos Reyes F S L, Lugtu E J, Manzano J A, Monton S N, Muñoz J E, Ong K D, Pilapil D Y, Roque V, Tan S M, Lim J A & Macabeo A P, *Comb Chem High Throug Screen*, 26 (2023), 459.

38 Shah A, Choudhary A, Jain M, Perumal S, Patel V, Parmar G & Patel A, *Biotech*, 14 (2024) 83.

39 Shah A & Seth A K, *Curr Drug Disc Tech*, 18 (2021) 75.

40 Muniyasamy R, & Manjubala I, *J Biomol Struc Dyn*, 42 (2024), 6588.

41 Shah A, Parmar G, & Seth A K, *Curr Comp Aid Drug Des*, 17 (2021), 344.

42 Fernandez R A, Quimque M T, Notarte K, Manzano J A, Pilapil D Y IV, de Leon V N, San Jose J J, Villalobos O, Muralidharan N H, Gromiha M M, Brogi S & Macabeo A P G, *J Biomol Struc Dyn*, 40 (2022) 12209.

43 Adasme M F, Linnemann K L, Bolz S N, Kaiser F, Salentin S, Haupt V J & Schroeder M, *Nucleic Acid Res*, 49 (2021) W530.

44 Dang J, Tiwari S K, Lichinchi G, Qin Y, Patil V S, Eroshkin A M & Rana T M, *Cell Stem Cell*, 19 (2016), 258.

45 Lanka G, Begum D, Banerjee S, Adhikari P Y & Ghosh B, *Comp Biol Med*, 166 (203) 107481.

46 Shah A, Parmar G, Shah U & Perumal S, *Chem Africa*, 6 (2023) 1847.

47 Labib B A & Chigbu D I, *Trop Med Infec Dis*, 7 (2022) 106.

48 Brogi S, Quimque M T, Notarte K I, Africa J G, Hernandez J B, Tan S M, Calderone V & Macabeo A P, *Comp (Basel)*, 10 (2022) 7.

49 Wang C, Gong X, Bo A, Zhang L, Zhang M, Zang E, Zhang C & Li M, *Molecule*, 25 (2020) 287.

50 Kushwaha P P, Singh A K, Bansal T, Yadav A, Prajapati K S, Shuaib M & Kumar S, *Front Cell Inf Microbiol*, 11 (2021) 2021.

51 Venditti A, Serrilli A M & Bianco A, *Nat Prod Res*, 27 (2013) 1413.

52 Vishvakarma V K, Pal S, Singh P & Bahadur I, *J Mol Struc*, 1251 (2022) 131965.

53 Krishnan V, Verma P, Saha S, Singh B, Vinutha T, Kumar R R, Kulshreshta A, Singh S P, Sathyavathi T, Sachdev A & Praveen S, *Biocat Agri Biotech*, 43 (2022) 102411.

54 Guo S, Bao L, Li C, Sun J, Zhao R & Cui X, *Sci Rep*, 10 (2020) 2020.

55 Vishvakarma V K, Singh M B, Jain P, Kumari K & Singh P, *Amino Acid*, 54 (2022) 205.

56 Kumari R & Kumar R, *J Chem Inform Model*, 54 (2014) 1951.

57 Abdou A, Maaghloud F E, Elmakssoudi A, Aboulmouhajir A, Eddine J, & Dakir M, *Nat Product Res*, 38(2024) 1099.

58 Prinsa, Saha S, Bulbul M Z H, Ozeki Y, Alamri M A & Kawsar S M A, *J Asian Nat Product Res*, 26 (2024) 955.

59 Kumar S, Dubey R, Mishra R, Gupta S, Dwivedi V D, Ray S, Jha N K, Verma D, Tsai L W & Dubey N K, *J Biomol Struc Dyn*, 7 (2024) 1.

60 Ahamad S, Gupta D & Kumar V, *J Biomol Struc Dyn*, 40 (2022) 2430.

61 Alamri M A, Prinsa, Kawsar S M A & Saha S, *Mol Div*, 2024 (2024) 1.

62 Shah U, Patel N, Patel M, Rohit S, Solanki N, Patel A, Patel S, Patel V, Patel R & Jawarkar R D, *Chem Biodiv*, 21 (2024) e202301903.

63 Daina A, Michielin O & Zoete V, *Sci Rep*, 7 (2017) 42717.

64 Prinsa & Saha S, *J Exper Bio Agri Sci*, 12 (2024) 800.

65 Quimque M T J, Notarte K I R, Fernandez R A T, Mendoza M AO, Liman R A D, Lim J A K & Macabeo A P G, *J Biomol Struc Dyn*, 39 (2021), 4316.

66 Saha S, Prinsa, Jakhmola V, Mahato A K, Ashok P K, Warikoo V & Mukhopadhay S, *Moroccan J Chem*, 11 (2023) 897.

67 Akter N, Saha S, Hossain M A, Uddin K M, Bhat A R, Ahmed S & Kawsar S M A, *Chem Phys Imp*, 9 (2024) 100700.

68 Saha S, Pal D & Nimse S B, *Current Drug Target*, 22 (2021) 1437.

69 Zhao L, Ciallella H L, Aleksunes L M, & Zhu H, *Drug Discov Today*, 25 (2020) 1624.

70 Akter S, Alhatlani B Y, Abdallah E M, Saha S, Ferdous J, Hossain M E, Ali F & Kawsar S M A, *Molecule*, 28 (2023) 8001.

71 Rochlani S, Bhatia M, Rathod S, Choudhari P & Dhavale R, *Nat Product Res*, 38 (2024) 891.

72 Yu J, Su N Q & Yang W, *JACS Au*, 2 (2022) 1383.

73 Kayes M R, Saha S, Alanazi M M, Ozeki Y, Pal D, Hadda T B, Legssyer A & Kawsar S M A, *Saudi Pharm J*, 31 (2023) 101804.

74 Harder E, Damm W, Maple J, Wu C, Reboul M, Xiang J Y, Wang L, Lupyan D, Dahlgren M K, Knight J L, Kaus J W, Cerutti D S, Krilov G, Jorgensen W L, Abel R, & Friesner R A, *J Chem Theory Comp*, 12 (2016) 281.

75 Kawsar S M A, Hossain M A, Saha S, Abdallah E M, Bhat A R, Ahmed S, Jamalis J, & Ozeki Y, *Chem Sel*, 9 (2024), 1.

76 Alamri M A, Alawam A S, Alshahrani M M, Kawsar S M A, Prinsa & Saha S, *Molecule*, 28 (2023) 5050.

77 Atiya A, Alhumaydhi F A, Shamsi A, Olatunde A, Alsagaby S A, Abdulmonem W, Sharaf S E & Shahwan M, *ACS Omega*, 7 (2022) 38361.

78 Kumari M, Singh R, & Subbarao N, *J Biomol Struc Dyn*, 40 (2022) 13497.

79 Almeleebia T M, Ahamad S, Ahmad I, Alshehri A, Alkhathami A G, Alshahrani M Y, Asiri M A, Saeed A, Siddiqui J A, Yadav D K & Saeed M, *Front Pharmacol*, 9 (2022) 847499.

80 Alharbi A S, Altwaim S A, El-Daly M M, Hassan A M, Al-Zahrani I A, Bajrai L H, Alsaady I M, Dwivedi V D & Azhar E I, *BMC Chem*, 18 (2024) 141.

81 Kuchana M & Kambala L B, *J Appl Pharm Sci*, 11 (2021) 031.

82 Jain A S, Sushma P, Dharmashekar C, Beelagi M S, Prasad S K, Shivamallu C, Prasad A, Syed A, Marraiki N & Prasad K S, *Saudi J Biol Sci*, 28 (2021) 1040.

83 Javid A & Ahmed M, *J Biomol Struc Dyn*, 42 (2024) 4578.

84 Wei C, Zhang H, Niu L, Zhong Q, Yan H & Wang J, *Comp Biol Chem*, 112 (2024) 108131.

85 Shahwan M, Hassan N, Ashames A, Alrouji M, Alhumaydhi F, Abdulmonem W, Muhsinah A B, Furkan M, Khan R H, Shamsi A & Atiya A, *Int J Biol Macromol*, 245 (2023) 125466.